High sensitivity of fluorine gas-assisted FIB-TOF-SIMS for chemical characterization of buried sublayers in thin films

Agnieszka Priebe[1,*], Laszlo Pethö[1], Emese Huszar[1,2], Tianle Xie[1,3], Ivo Utke[1] and Johann Michler[1]

[1]Empa, Swiss Federal Laboratories for Materials Science and Technology, Laboratory for Mechanics of Materials and Nanostructures, Feuerwerkerstrasse 39, CH-3602 Thun, Switzerland

[2]Laboratory for Nanometallurgy, Department of Materials, ETH Zurich, Vladimir-Prelog-Weg 5, 8093, Zurich, Switzerland

[3]College of Material Science and Engineering, Hunan University, 2 Lushan S Rd, Yuelu, Changsha, 410082, P.R. China

KEYWORDS: thin films, elements, chemical structure, chemical characterization, TOF-SIMS, sensitivity

ABSTRACT: In this work, we present the potential of high vacuum-compatible time-of-flight secondary ion mass spectrometry (TOF-SIMS) detectors, which can be integrated within focused ion beam (FIB) instruments, for precise and fast chemical characterization of thin films buried deep under sample surface. This is demonstrated on complex multilayer systems composed of alternating ceramic and metallic layers with thicknesses varying from several nanometers to hundreds of nanometers. The typical problems of TOF-SIMS technique, i.e. low secondary ion signals and mass interference between ions having similar masses, were solved using a novel approach of co-injecting fluorine gas during sample surface sputtering. In the most extreme case of $Al/Al_2O_3/Al/Al_2O_3/.../Al$ sample, a <10 nm thick Al_2O_3 thin film, buried under 0.5 μm material, was detected and spatially resolved using only $^{27}Al^+$ signal distribution. This is an impressive achievement taking into account that Al and Al_2O_3 layers varied only by the small amount of oxygen content. Due to its high sensitivity, fluorine gas-assisted FIB-TOF-SIMS can be used for quality control of nano- and microdevices as well as for the failure analysis of fabrication processes. Therefore, it is expected to play an important role in the development of microelectronics and thin film-based devices for energy applications.

INTRODUCTION

Thin films are defined as 2D layers (i.e. they have one dimension negligible when compared to the two other dimensions), which are deposited by a progressive addition of atoms or molecules.[1,2] Usually their thicknesses vary between subnanometres and several micrometres. The specific structure of thin films allows them to achieve properties, which are not accessible by their bulk material. Therefore, they are commonly used to improve the surface properties of solids[3], such as hardness[4] (for watches, jewellery and decorative items), reflection or resistance to corrosion[5]. Furthermore, thin films find many applications in microelectronics for high-k dielectrics[6], microbatteries for new energy devices[7–10], solid oxide fuel cells (SOFC)[11], in fabrication of $Cu(In,Ga)Se_2$ thin film solar cells[12–14], Dye-Sensitized Solar Cells (DSSCs), photovoltaics, organic photovoltaics, transparent conducting oxides[15] (TCOs, such as SnO_2, ZnO, Al:ZnO, black silicon)[16–19], anti-reflective coatings[15], thin film electroluminescent (TFEL) displays[20], thin film metal–oxide–semiconductor field-effect transistor (MOSFET)[21], micro- and nano-electromechanical systems (MEMS[22] and NEMS[23]), light-emitting diodes (LEDs)[24] as well as in medical applications[25] and aerospace[26].

The extensive advances of multilayer systems composed of thin films, which are often buried deep in a bulk material, imply a strong demand for precise and reliable chemical characterization techniques providing nanoscale resolution. This is a challenging task as most of the conventional methods do not have sufficient depth resolution (Energy-Dispersive X-ray Spectroscopy, EDX), the analysis region is very small, and thus might not be representative for the entire specimen (Atom Probe Tomography, APT[27] and Scanning Transmission Electron Microscope, STEM[28], combined with EDX) and/or the sample preparation process is very time-consuming and often requires additional instrumentation (such as Focused Ion Beam, FIB[29]). A powerful alternative to the aforementioned techniques is Time-Of-Flight Secondary Ion Mass Spectrometry (TOF-SIMS)[30,31], which allows a sample structure to be chemically characterized in 3D with nanoscale spatial resolution[32,33], and high mass resolution. All (light and heavy) ionized atoms and molecules can be detected and isotopes can be recognized. This is an important feature when compared to STEM/EDX, which does not enable light elements, such as Li (broadly used in solid state microbatteries), to be detected. The detailed comparison of these two techniques is

presented in our previous work[34]. Although Li mapping can be achieved with atomic resolution when combining STEM with EELS (electron energy loss spectroscopy), this solution is challenging[35] and requires tedious lamellae preparation.

Furthermore, the extraordinary TOF-SIMS sensitivity[36] in the order of ppm-ppb allows even trace elements to be measured. The size of the analysed Region-Of-Interest (ROI) can be as small as $1\mu m \times 1\mu m$ and as large as $400\mu m \times 400\mu m$, providing complete information on sample composition. TOF-SIMS does not require any sample preparation (sample surface should be flat[37] and preferably conductive), which is an important advantage over STEM/EDX allowing for optimization of experiment duration and costs. Furthermore, a high vacuum (HV) compatible TOF detector[33,38,39] can be integrated within a FIB analytical chamber, which enables *insitu* correlative studies with other techniques such as Scanning Electron Microscopy (SEM), Atomic Force Microscopy (AFM), EDX, Electron Backscatter Diffraction (EBSD), Raman spectroscopy as well as exploitation of Gas Injection System (GIS) to be conducted without breaking vacuum conditions between the measurements.

The operation of HV-compatible TOF-SIMS add-on (such as HTOF from TOFWERK) integrated within FIB/SEM is quite different than the operation of dedicated TOF-SIMS instrument (such as TOF.SIMS5 from IONTOF) working under ultra-high vacuum (UHV) conditions. In the case of HTOF, a single continuous primary ion beam (so far, usually a Ga beam but other beams such as Ne, He, Xe, O, N etc. can potentially be also applied) is used for both, sputtering and analysis, and then the secondary ion beam is pulsed, whilst TOF.SIMS5 is a dual source system with a pulsed Bi_n primary ion beam used for imaging and a separate pulsed O_2, Cs, Ar or Xe beam used for sputtering. The enhancement of secondary ion generation can be achieved by co-injection of supplementary gases provided by GIS (H_2O or XeF_2) in the case of HTOF, whilst the effect of species forming a sputtering beam (O_2 or Cs) and/or O_2 flooding is used to increase ion yields in the case of TOF.SIMS5. Furthermore, the HTOF optics is not optimal as it has to fit to an existing FIB/SEM (usually equipped with other analytical techniques) whilst TOF.SIMS5 is a standalone instrument. The detector specifications indicate the lateral resolution <50 nm for HTOF working with Ga beam and <60 nm for TOF.SIMS5. In the case of depth resolution, <20 nm is reported for HTOF and <1 nm for TOF.SIMS5. However, the literature shows that significantly higher spatial resolution of both instruments can be achieved when specialized procedures are implemented. The mass resolution can vary between 3000 and 7000 for HTOF and is >10000 for TOF.SIMS5. Finally, the operation under HV and UHV can have advantages and disadvantages. On the one hand the contamination of a sample surface from residual gas is lower under UHV, but on the other hand the presence of oxygen ions can have beneficial effect on the ionization efficiency during the experiments under HV. Overall, the

beam type (element type, single ions/clusters), primary ion beam parameters (energy, current), chemical state (without/with supplementary gases) determine the performance of the TOF-SIMS technique and the most optimal experimental conditions vary depending on analysed materials. To the best of our knowledge, there are no systematic studies, which compare full potential and limitations of these two types of TOF-SIMS instruments. Only two studies, showing elemental images obtained with the HV-compatible TOF-SIMS add-on and the dedicated UHV TOF-SIMS instrument, which were conducted on exactly the same samples and compared to STEM/EDX results, have been published[34,40].

In this work, we present the very high chemical sensitivity of Ga+ HV FIB-TOF-SIMS for chemical characterization of 1-10 nanometre thick ceramic thin films (Al_2O_3) buried between tens to hundreds of nanometre thick metallic layers (Al, Ni, Cu, Zr, Mo, Ag, Au and ZrMoAg). Our studies show that the spatial resolution, and thus the image quality of the thin films can be significantly improved by the novel combination of FIB-TOF-SIMS with *in situ* GIS, which allowed fluorine gas to be simultaneously delivered to sample surfaces. In the most extreme case of $Al/Al_2O_3/Al/Al_2O_3/.../Al$ sample, an approx. 8.5 nm thick Al_2O_3 thin film, buried around 530 nm deep below the surface, was detected and spatially resolved using only the distribution of a single secondary ion signal. This is an important achievement taking into account the very small size of ceramic thin films and the fact that the chemical structure of the alternating layers varied only by the oxygen content.

EXPERIMENTAL

Materials

A set of three state-of-the-art multilayer model samples was fabricated using an innovative hybrid system combining physical vapor deposition (PVD) and atomic layer deposition (ALD)[20], which allows subsequent deposition processes to be conducted without breaking vacuum conditions. This was an important technological advance (as, so far, the PVD and ALD processes were performed in separate vacuum chambers [41,42]) allowing the layers' surface oxidation to be avoided, and multilayer production costs to be significantly reduced. Moreover, the combination of ALD and PVD provided us a unique opportunity of depositing multilayers composed of thin films with thicknesses varying by up to two orders of magnitude. A detailed description of the custom-made ALD-PVD instrument (designed at Empa, Thun, Switzerland and fabricated by MANTIS Deposition Ltd. Oxfordshire, United Kingdom) used in this study is presented in ref.[43]. The high purity (99.95%-99.99%) metal targets from HMV Hauner (Roettenbach, Germany) and Testbourne Ltd (Basingstoke, United Kingdom), were used for the thin film depositions.

The multilayer stacks consisted of alternating metallic thin films with thicknesses in the order of 10-100 nm (deposited
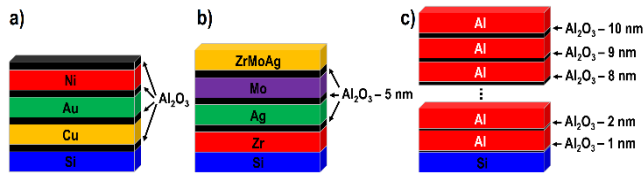
Figure 1. Diagram of dedicated model samples fabricated with hybrid ALD-PVD: a) $Al_2O_3/Ni/Al_2O_3/Au/Al_2O_3/Cu/Al_2O_3$, b) $ZrMoAg/Al_2O_3/Mo/Al_2O_3/Ag/Al_2O_3/Zr$, c) $Al/Al_2O_3/Al/Al_2O_3/.../Al$. Not to scale.

with PVD) and ceramic thin films with the thicknesses varying from 1 to 10 nm (deposited with ALD). The diagrams of the model multilayers are given in Figure 1. The $Al_2O_3/Ni/Al_2O_3/Au/Al_2O_3/Cu/Al_2O_3$ multilayer was fabricated to verify the feasibility of measuring insulating layers buried in a conducting material. In this case, the sample components were chosen to ensure a high mass (precisely mass-to-charge ratio, $\left(\frac{m}{Q}\right)$) contrast between the layers (i.e. $\left(\frac{m}{Q}\right)_{Al} = 27$, $\left(\frac{m}{Q}\right)_{Ni} = 58$, $\left(\frac{m}{Q}\right)_{Au} = 197$ and $\left(\frac{m}{Q}\right)_{Cu} = 63$) and, therefore, reduce the probability of artefacts originating from potential mass interference. Furthermore, the differences in sputtering rates between metallic and ceramic components were analyzed to design an optimal structure of the final model sample for demonstrating the very high sensitivity of FIB-TOF-SIMS. This sample was also used to optimize the experimental conditions, such as primary ion beam current, for measurements at low beam energy of 5 keV (used for the final model sample). The design of $ZrMoAg/Al_2O_3/Mo/Al_2O_3/Ag/Al_2O_3/Zr$ multilayer was based on approx. 100 nm thick metallic PVD layers separated by approx. 5 nm thick ceramic ALD layers. The PVD layers consisted of metals, whose combination of secondary ions can result in high mass-interference (for example TOF-SIMS signal acquired at mass 98 corresponds to $^{98}Mo^+$ ions and $^{96}Zr^1H_2^+$ ions whilst $^{107}Ag^+$ ions have the same mass as $^{91}Zr^{16}O^+$ ions), to demonstrate the benefits of conducting fluorine gas-assisted TOF-SIMS analysis. Finally, in the case of $Al/Al_2O_3/Al/Al_2O_3/.../Al$ multilayer, the deposition parameters were adjusted to provide eleven approx. 125 nm thick Al thin films separated with ten Al_2O_3 thin films with thicknesses varying between 1 nm (the layer deposited the closest to the substrate) and 10 nm (the layer located the closest to the multilayer surface) with 1 nm size increment. The precise thicknesses of Al_2O_3 layers were achieved due to the self-limiting nature of the ALD process. This was proven in our previous paper[43] using TEM. Al was chosen as the main sample component in this case as it is characterized with excellent ionization efficiency and low detection limits[40,44,45]. Since the PVD and ALD layers differed between each other only by the presence of oxygen content, this sample was used for presenting the extremely high sensitivity of FIB-TOF-SIMS technique. The exact deposition parameters of model samples are summarized in Table S1-S6. A <100> single crystal Si wafer was used as a substrate for all multilayers. A Tepla Ion80 RF plasma sputtering instrument was used to clean the substrate surface prior the deposition in the case of $ZrMoAg/Al_2O_3/Mo/Al_2O_3/Ag/Al_2O_3/Zr$ multilayer.

Methods

A Hitachi (Tokyo, Japan) S-4800 high resolution Field Emission Scanning Electron Microscope (FE-SEM)[46] was used to image the cross-sections of the multilayers and measure the exact thicknesses of the thin films.

The elemental characterization was conducted using a HV-compatible High Resolution TOF (HTOF) detector from TOFWERK (Thun, Switzerland) integrated within a FIB/SEM dual beam system LYRA3 from Tescan (Brno, the Czech Republic). The supplementary fluorine gas was provided by an *in situ* GIS. In this study, we present for the first time combination of HTOF with GIS. Compared to the Compact TOF (CTOF), which is reported in our previous publications[47–49], the front part of HTOF optics is different and the detector column is located much closer to a sample surface. In this case, the nominal location of GIS nozzle (i.e. the location that is usually used for standard GIS applications such as material deposition or increase of FIB sputter rates) distorts applied electric field lines between a sample surface and the tip of the TOF detector, consequently preventing efficient ion collection. Therefore, an adjustment of GIS location was performed on a bulk Si sample prior to the actual measurements on the multilayers. The maximum efficiency of ion collection was achieved when GIS was withdrawn by around 1.4 mm with respect to the nominal configuration (i.e. 23 mm instead of 24.4 mm in the case of this setup). Most likely, such modification of the GIS position results in a different quantity of delivered gas to the sample surface and, consequently, can influence the sputtering and ionization processes differently than in the case of using the CTOF detector. The samples were measured at standard vacuum conditions (without any gas, i.e. at approx. 6×10^{-6} mbar chamber background pressure) and in the presence of XeF_2 (i.e. at approx. 8×10^{-6} mbar chamber background pressure). During gas-assisted TOF-SIMS, the changes of ionization probability of sample components are rather assigned to the presence of F than Xe, as Xe is noble gas. However, the influence of the Xe cannot be completely excluded at this stage. The amount of delivered gas cannot be measured directly during the TOF-SIMS experiments. However, the gas flux can be simulated, as we have presented in detail in our previous work.[47,50]

A continuous (i.e. not pulsed) mono-isotopic $^{69}Ga^+$ FIB beam was used for sputtering and imaging during the TOF-SIMS analysis. The $Al_2O_3/Ni/Al_2O_3/Au/Al_2O_3/Cu/Al_2O_3$ and $Al/Al_2O_3/Al/Al_2O_3/.../Al$ multilayers were measured at 5 keV energy beam and 51-54 pA ion current to maximize the depth resolution at standard vacuum conditions. The $ZrMoAg/Al_2O_3/Mo/Al_2O_3/Ag/Al_2O_3/Zr$ sample was measured with a 20 keV energy beam at 117-118 pA ion current. This allowed us to demonstrate that high quality elemental images can be obtained at high beam energy (setting the instrument at higher beam energies is usually much faster and easier than setting it at low beam energies) in the presence of supplementary gas. In the case of all samples, the signal was collected with 32 µs dwell time from 10µm×10µm

areas with 512×512 pixels and 2×2 binning. In order to prevent data acquisition artefacts, the elemental images and depth profiles were generated using only the central 5μm×5μm ROI. The data was mass-calibrated with the most prominent isotope peaks of the samples, the sample substrate ($^{28}Si^+$) and the primary ion beam ($^{69}Ga^+$). The data acquisition and processing were done using Tof-Sims Explorer 1.4.0.0 with TofDaq version 1.99 (from TOFWERK, Thun, Switzerland).

Results and discussion

The main objective of this work is to demonstrate the extreme sensitivity of FIB-TOF-SIMS technique for characterizing complex material structures based on thin films. To achieve that, we launched systematic studies on different multilayers with increasing complexity of their structures. The exact composition and thicknesses of the thin films were achieved thanks to the *in situ* hybrid ALD-PVD system, which enabled all crucial (for this study) elements to be deposited with high precision. In the first step of this study, a conductive-insulating multilayer sample ($Al_2O_3/Ni/Al_2O_3/Au/Al_2O_3/Cu/Al_2O_3$), which consisted of elements ensuring high material contrast and, therefore, preventing potential mass interference, was designed. The feasibility of imaging the ceramic ALD thin films buried between metallic PVD layers was verified. Furthermore, the differences in sputtering rates were analysed. In the following stage, we designed a multilayer structure consisting of metals, whose secondary ion signals highly mass interfere and, therefore, are difficult to characterize with TOF-SIMS under standard vacuum conditions. This sample was used to present the benefits of conducting fluorine gas-assisted TOF-SIMS analysis, which allows mass interference to be separated. The obtained results also demonstrate the potential of FIB-TOF-SIMS for the quality verification of multilayer deposition process and the failure analysis. In the final step, the very high sensitivity of FIB-TOF-SIMS was proved using a dedicated model multilayer, whose thin films' chemical structure varied only by the presence of oxygen content (i.e. $Al/Al_2O_3/Al/Al_2O_3/.../Al$).

SEM and TEM imaging on the sample cross-sections and layer thickness measurements

Figure S1 shows the SEM images acquired on the sample cross-sections, which were mechanically cleaved. The total thickness of 186 nm was measured in the case of $Al_2O_3/Ni/Al_2O_3/Au/Al_2O_3/Cu/Al_2O_3$. Due to insufficient image resolution and contrast as well as the surface of the cross-section, the thicknesses of individual Ni, Au and Cu layers could not be assessed. However, in the case of two other two samples, the PVD thin films were distinct and their size in the order of 100 nm was measured. It was not possible, though, to distinguish any Al_2O_3 layers using SEM imaging. As the exact size of these layers was crucial for determining FIB-TOF-SIMS sensitivity, supplementary

TEM imaging of $Al/Al_2O_3/Al/Al_2O_3/.../Al$ lamellae was provided (Figure S2). The thickness of 10th and 8th (counting from the substrate) Al_2O_3 thin film was 12.1 nm and 9.7 nm, respectively. This allowed the size of 7th layer (the deepest buried thin film, which was measured with TOF-SIMS) to be calculated (approx. 8.5 nm).

FIB-TOF-SIMS elemental characterization of multilayer structure composed of conducting and insulating thin films

The TOF-SIMS technique provides 4D data sets consisting of *x*-, *y*- and *z*-coordinates with an associated mass spectrum for each acquisition point. In the case of multilayers, whose components are uniformly distributed in the lateral plane, usually the chemical images in depth (i.e. the *x-z* plane with signal integration in the *y*-direction) are used to verify the quality of the thin films. Figure 2 shows the chemical structure of $Al_2O_3/Ni/Al_2O_3/Au/Al_2O_3/Cu/Al_2O_3$ multilayer sample based on the main isotope ($^{27}Al^+$, $^{28}Si^+$, $^{58}Ni^+$, $^{63}Cu^+$ and $^{197}Au^+$) signal distributions. Despite different ionization efficiencies, all elements provided sufficiently high secondary ion signals to enable for layer representation in 2D and recognition of interfaces between them. Furthermore, the TOF-SIMS chemical images, in conjunction with SEM surface imaging of the FIB-sputtered crater, show a lack of the Ga^+ beam drift during the data acquisition, which was one of the main concerns regarding the measurements of multilayers containing insulating thin films. The obtained TOF-SIMS data indicate that both, ALD and PVD processes were conducted precisely providing smooth homogenous thin films. No pores, material segregation or material diffusion were observed. In the case of the experiments performed under standard vacuum conditions (Figure 2a), the $^{27}Al^+$ secondary ion signal is the highest among all considered signals although the Al content in the sample is the lowest. As aforementioned, this is due to the excellent ionization efficiency of Al. Furthermore, the Al ion yields can be potentially increased in this case due to the presence of oxygen (matrix effect[51–53]), which is a well-known element for enhancing the generation of positive ions[31,54,55]. Although Si constitutes only the sample substrate, the secondary ion signal at mass 28 is also detected at the location of ALD layers. This does not represent the real presence of Si in these layers but results from the mass interference between the most prominent isotope of Si, $^{28}Si^+$, and $^{27}Al^1H^+$ ions. Commonly, the presence of mass interference is verified by comparing the measured isotope abundance with the natural isotope abundance of the studied element[48,49,56]. Regarding sputtering rates, *S*, ceramics are not milled as efficiently as pure metals. For comparison, $S_{Al_2O_3}$=0.08 μm³/nC, S_{Cu}=0.25 μm³/nC, S_{Ni}=0.14 μm³/nC and S_{Au}=1.50 μm³/nC for Al_2O_3, Cu, Ni and Au, respectively in the case of 30 keV Ga^+ FIB under normal incidence[57]. Therefore, the Al_2O_3 layers, whose thicknesses are one or two orders of magnitude smaller than the thicknesses of the metal layers, can be still precisely represented during FIB-TOF-SIMS chemical imaging.
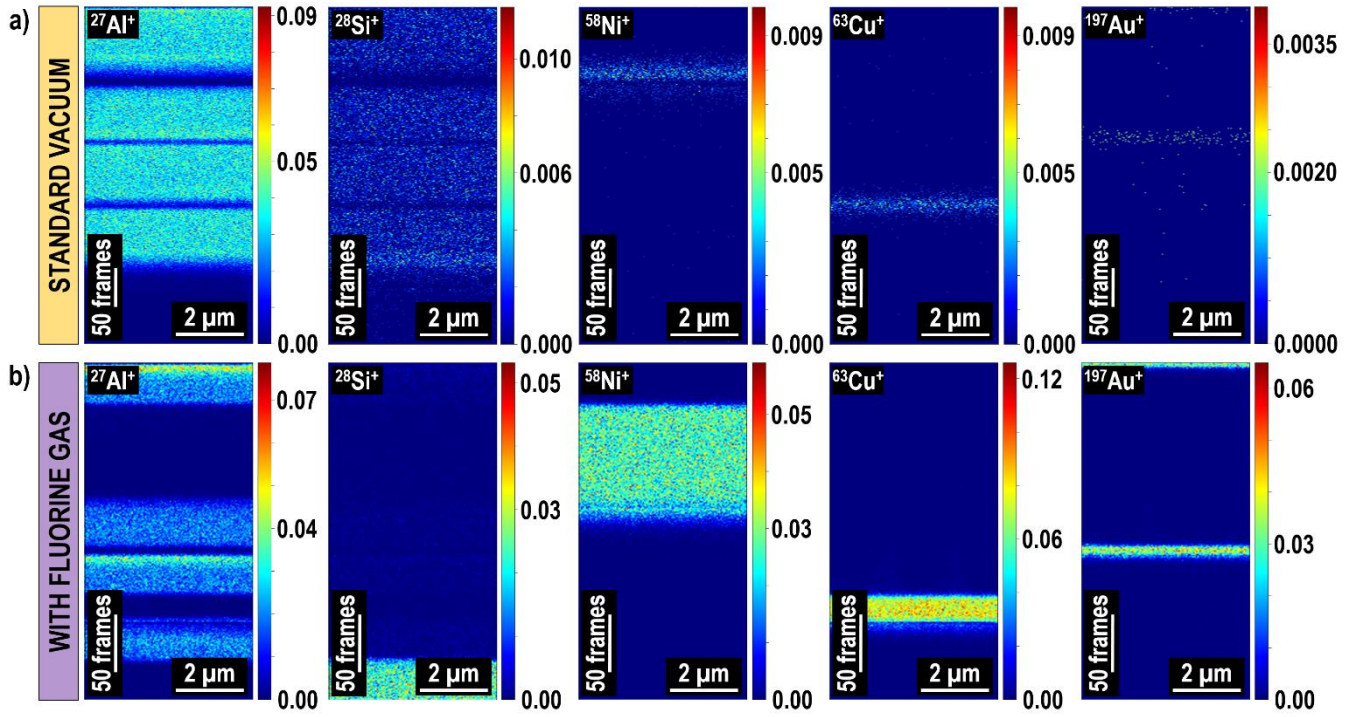
Figure 2. 2D elemental images of the $Al_2O_3/Ni/Al_2O_3/Au/Al_2O_3/Cu/Al_2O_3$ sample. The signals of the most prominent isotopes are presented in x-z plane (i.e. in depth; integration in y-direction). The z-dimension is given as a number of frames, i.e. acquisition scans, where 1 frame corresponds to approx. 10.24 s of the sputtering time. The colour scale is given in counts per extraction. The TOF-SIMS results were obtained under standard vacuum conditions (a) and in the presence of fluorine gas (b). The time needed to measure the multilayer (i.e. to reach the Si substrate) was approx. 58 min and 44 min, respectively.

Recently, combining HV-compatible TOF detectors with in situ GIS has been developed allowing for a gas-assisted TOF-SIMS analysis[47–49]. This innovative approach demonstrates a great potential for enhancing secondary ion generation, which consequently can lead to higher spatial resolution. So far very promising results were obtained during the experiments with H_2O and XeF_2 gas precursors and potentially this solution allows many other gases to be efficiently delivered to a sample surface. Furthermore, in the case of some elements, it was observed that simultaneous fluorine gas co-injecting can induce separation of mass interference[48]. This is an important methodological advance, as so far mass interference was one of the major drawbacks of the TOF-SIMS technique. Figure 2b shows the elemental images of the $Al_2O_3/Ni/Al_2O_3/Au/Al_2O_3/Cu/Al_2O_3$ acquired in the presence of fluorine gas. The secondary ion signals of the metal layers are significantly enhanced providing better recognition of interfaces locations. Moreover, the $^{28}Si^+$ signal distribution does not follow the same pattern as $^{27}Al^+$ signal distribution (in contrast to the results obtained under standard vacuum conditions, Figure 2a). This indicates the fluorine gas-induced separation of mass interference between $^{28}Si^+$ and $^{27}Al^1H^+$, which most likely results from different influence of F on Al and Si ionization efficiencies as well as modifications in formation of hydrides[48]. Consequently, more representative TOF-SIMS data (with respect to the sample composition) is provided in this case. The sputtering rates of all layers were modified due to the use of the supplementary gas. Among all considered materials, Ni was sputtered the slowest when compared to the results obtained under standard vacuum conditions.

Depth profiling is another way to represent TOF-SIMS data. Usually it is used when global information on a sample structure matters and local composition variations are not important for the analysis. Its use can also be beneficial when a count rate is too low for 2D or 3D imaging. In this case, a secondary ion signal is integrated over the x-y plane, and given as a function of sputtering time or number of acquired frames/scans. Directly from the TOF-SIMS measurements it is not possible to access the information on the amount of milled material unless the sputtering rates are known (which is not the case of novel materials). The depth of FIB-sputtered crater can be measured using SEM or AFM. However, the latter one demands time-consuming and demanding protocols to assess thicknesses of individual thin films in the case of multilayer systems[58–60]. Figure S3 shows $Al_2O_3/Ni/Al_2O_3/Au/Al_2O_3/Cu/Al_2O_3$ depth profiles. The generation of $^{28}Si^+$, $^{58}Ni^+$, $^{63}Cu^+$ and $^{197}Au^+$ ions was significantly increased (up to over two orders of magnitude) due to the presence of fluorine gas. Interestingly, $^{27}Al^+$ signals coming from Al_2O_3 layers were slightly decreased (see also the detailed analysis of $Al/Al_2O_3/Al/Al_2O_3/.../Al$ sample discussed in the following sections of this work).

The normalization of depth profiles to 1 can be very helpful in the case of significant differences in ionization efficiencies between various sample components. Moreover, this

solution is usually used to estimate the location of interfaces between the sample layers[47-49], which allows ion yields, sputter rates and gas enhancement factors to be calculated. Figure S4 shows that the simultaneous co-injection of fluorine gas during the TOF-SIMS measurement provided statistically better results (when compared to the data obtained under standard vacuum conditions) due to the higher count rates, and therefore, lower signal fluctuations. The shape of the $^{27}Al^+$ signal distribution indicates much stronger dependency of Al ionization efficiency on the presence of neighbouring metallic layers, i.e. matrix effect than in the case of measurements without supplementary gas. This shows that despite the advantages of applying fluorine gas during a TOF-SIMS analysis, reference measurements under standard vacuum conditions should be performed for comparison.

Co-injection of fluorine gas during TOF-SIMS analysis as a solution for mass interference problem: enhancement of spatial resolution and improvement of layer recognition

The technology of microelectronics and new thin film-based devices for energy applications very often relies on materials made of elements coming from narrow regions of periodic table. This means that separate device components can be built of elements having very similar isotopes' mass-to-charge ratios. For example CIGS thin film solar cells[61] are based on Cu ($\left(\frac{m}{Q}\right)_{Cu}$ =63 and 65), Zn ($\left(\frac{m}{Q}\right)_{Zn}$ =64, 66, 67, 68 and 70), Ga ($\left(\frac{m}{Q}\right)_{Ga}$ =69 and 71), Se ($\left(\frac{m}{Q}\right)_{Se}$ =74, 76, 77, 78, 80 and 82), Mo ($\left(\frac{m}{Q}\right)_{Mo}$ =92, 94, 95, 96, 97, 98 and 100), Cd ($\left(\frac{m}{Q}\right)_{Cd}$ =106, 108, 110, 111, 112, 113, 114 and 116) and In ($\left(\frac{m}{Q}\right)_{In}$ =113 and 116). In general, such a configuration is not optimal for a TOF-SIMS analysis due to the potential mass interference (usually between different element isotopes or their hydrides and oxides), which can prevent proper element distributions to be assessed. In the case of poly-isotopic elements, whose main isotope signal is biased with mass interference, another isotope's signal can be potentially used. Nevertheless, very often the signal-to-noise ratios of non-dominant isotopes are insufficient. Although in the case of dedicated TOF-SIMS instruments (such as TOF.SIMS5 from IONTOF), which use a pulsed primary ion beam, the mass resolution can be increased by decreasing the pulse duration[37,62,63], this results in the degradation of the spatial resolution. Furthermore, the mass resolution of detectors using a continuous analysis ion beam (as presented in this work) is fixed and cannot be easily modified. The presence of mass interference can be verified by comparing the measured isotope abundance to the natural isotope abundance. However, this is not possible in the case of elements having single isotopes, such as Be, Na, Al, Sc, Mn, Co, As, Y, Nb, Rh etc. Therefore, the mass interference is considered as one of the main drawbacks of the TOF-SIMS technique.

As mentioned, co-injection of fluorine gas during FIB sputtering can lead to the separation of mass interference[48]. In the former section, the separation of secondary ion signals coming from $^{27}Al^1H^+$ and $^{28}Si^+$ was shown. In this case the presence of the mass interference can be easily recognized based on the initial knowledge of the sample composition, i.e. Si forms only the substrate. However, the situation becomes much more difficult when the main body of a sample is built of elements whose isotopes, hydrides or oxides are similar. To show the potential of fluorine-gas assisted FIB-TOF-SIMS analysis, we have designed and fabricated a multilayer structure consisting of Zr, Mo and Ag, whose combination of ion signals provides a very complex mass interference problem. For example, signal acquired at mass 107 can originate from $^{107}Ag^+$ ions as well as $^{91}Zr^{16}O^+$ ions. Furthermore, signals measured at masses 92, 94 and 96 can come from both, Zr and Mo isotopes. Besides, signals associated with Mo isotopes (^{92}Mo, ^{95}Mo and ^{97}Mo) can be biased with mass overlap coming from Zr hydrides ($^{91}Zr^1H$, $^{94}Zr^1H$ and $^{96}Zr^1H$, correspondingly). Finally, the mass interference can appear within signals originating from the element isotopes and their hydrides, for example between $^{90}Zr^1H$ and ^{91}Zr, between $^{91}Zr^1H$ and ^{92}Zr, between $^{94}Mo^1H$ and ^{95}Mo etc.

The elemental images and corresponding depth profiles of the ZrMoAg/Al$_2$O$_3$/Mo/Al$_2$O$_3$/Ag/Al$_2$O$_3$/Zr multilayer is presented using the $^{27}Al^+$, $^{28}Si^+$, $^{90}Zr^+$, $^{98}Mo^+$ and $^{107}Ag^+$ secondary ion signals, in Figure 3 and S6. The data, acquired under standard vacuum conditions (Figure 3a and S6a), show the detection of signal at mass 107, corresponding to $^{107}Ag^+$ ions, not only at the locations of the Ag and ZrMoAg layers but also at the location of the Zr layer. In the latter case, this observation could potentially lead to an incorrect conclusion that the Zr and Ag layers mixed during or after the thin film deposition. The first argument against this scenario is the presence of the Al$_2$O$_3$ barrier layer between these thin films. This can be not convincing enough in the view of the possibility of ALD deposition failure (discussed in the next section). However, knowing that $^{91}Zr^{16}O^+$ ions and $^{107}Ag^+$ ions have almost the same masses, it becomes clear that a strong mass-interference between them is the actual reason of detecting the TOF-SIMS signal at mass 107 within the Zr layer. The mass difference between $^{107}Ag^+$ and $^{91}Zr^{16}O^+$ ions is 0.0045 m/Q (i.e. 106.9051 m/Q vs. 106.9006 m/Q). This implies the necessity of the detector's mass resolution, $m/\Delta m$, of approximately 27000 to distinguish them. This is far beyond the capability of HTOF detector, whose $m/\Delta m$ =4710 at mass 107, in this case. Remarkably, this problem can be solved by co-injecting fluorine gas during the TOF-SIMS analysis as the response to the presence of supplementary gas is specific for individual elements[47-49]. Our previous studies on pure metallic thin films[47] show the enhancement of Ag ionization probability by a factor of 350 when fluorine gas was simultaneously delivered to the sample surface. Interestingly, under the same experimental
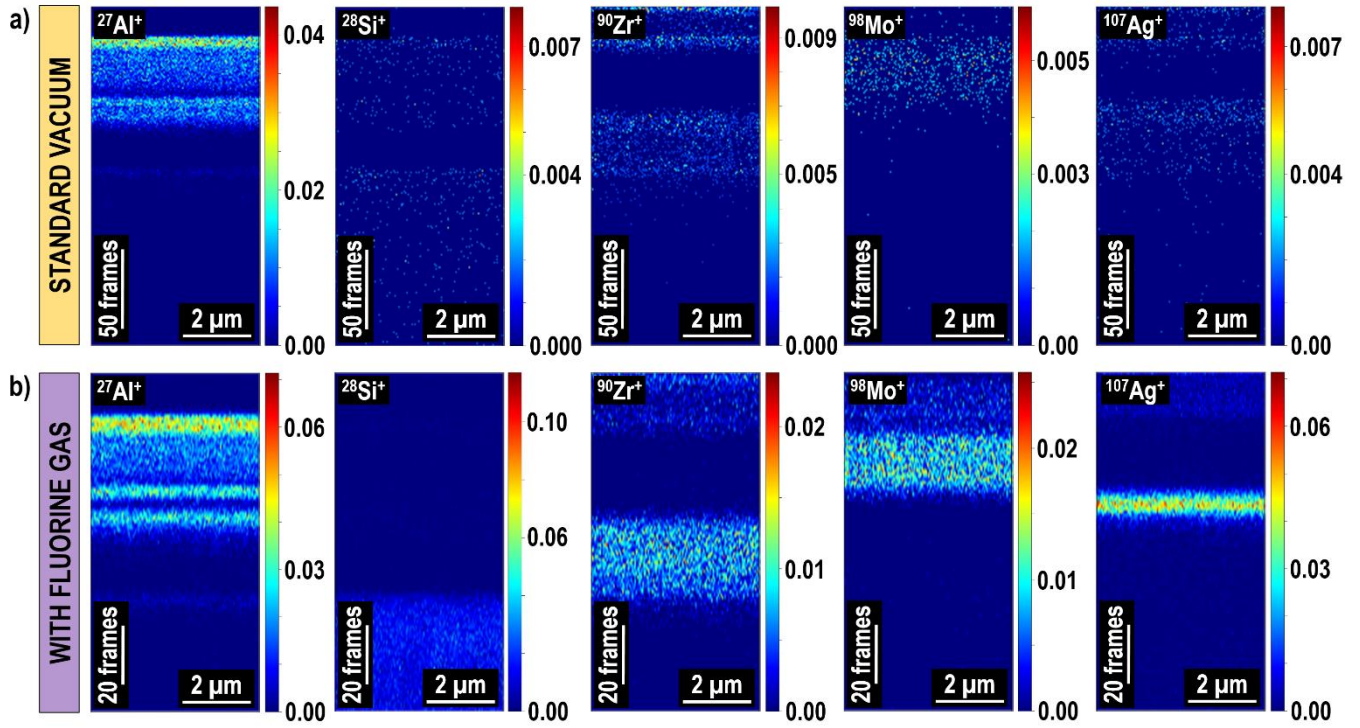
Figure 3. The elemental images of the ZrMoAg/Al$_2$O$_3$/Mo/Al$_2$O$_3$/Ag/Al$_2$O$_3$/Zr multilayer obtained under standard vacuum conditions (a) and in the presence of fluorine gas (b). The measurement duration (i.e. time needed to reach the Si substrate) was 18 min and 13 min, respectively. The ^{27}Al$^+$ signal distribution indicates failure of the ALD-PVD process as ^{27}Al$^+$ signal is detected outside the Al$_2$O$_3$ layers, i.e. at the location of the Mo layer. Note that the signal measured at mass 28, corresponding to ^{28}Si$^+$ ions, shows also the distribution of ^{27}Al^{1}H$^+$ ions in the case of data obtained under standard vacuum conditions (a).

conditions, the Zr secondary ion generation decreased by 27% when compared to the results obtained without any gas (in the case of experiments performed with CTOF). Fluorine has higher electron affinity than oxygen (322 kJ/mol vs. 141 kJ/mol)[64] and, therefore, can modify metal-oxygen interactions, potentially resulting in lower generation of metal oxide ions. In conclusion, these two mechanisms can lead to the fluorine gas-induced separation of mass interference during the TOF-SIMS analysis. As shown in Figure S5b and S6b, the shape of ^{107}Ag$^+$ signal distribution is independent from the shape of ^{90}Zr$^+$ signal distribution in the case of fluorine gas-assisted measurements. To support this statement, the comparison of signals acquired at masses 90, 106 and 107 (corresponding to ^{90}Zr$^+$, ^{90}Zr^{16}O$^+$ and ^{91}Zr^{16}O$^+$/^{107}Ag$^+$, respectively) is provided in Figure S7. In the case of experiments conducted under standard vacuum conditions (Figure S7a), ^{90}Zr$^+$ and ^{90}Zr^{16}O$^+$ signals follow the same pattern, whilst the signal measured at mass 107 indicates contribution of both ^{91}Zr^{16}O$^+$ and ^{107}Ag$^+$ ion signals. However, this signal in the presence of fluorine gas (Figure S7b) is independent from ^{90}Zr$^+$ and ^{90}Zr^{16}O$^+$ signals and appears only at the locations of ZrMoAg and Ag thin films. These results prove that the signal at mass 107 observed at the location of the Zr layer during the measurements conducted under standard vacuum conditions (Figure S6a) originated exclusively from the mass interference between ^{91}Zr^{16}O$^+$ ions and ^{107}Ag$^+$, and did not result from the mixing of Zr and Ag layers. Interestingly, the ^{90}Zr^{16}O$^+$ signal measured during fluorine-gas assisted TOF-SIMS does not follow exactly the same pattern as ^{90}Zr$^+$ signal. The

comparison of Figures S6b and S7b indicates that this can result from the contribution of Al-containing ions to the signal measured at m/Q=106, different matrix effect at the thin film interfaces and/or different influence of fluorine on formation of metal ions and metal oxide ions.

FIB-TOF-SIMS as a technique for deposition failure analysis and quality control

Due to the aforementioned high sensitivity and, therefore, the capability of detecting trace elements, the TOF-SIMS technique shows great potential for verifying the PVD-ALD process quality and the failure analysis. Figure 3 shows homogeneous distribution of all analysed elements in the lateral plane of the thin films. This means a lack of transverse material segregation. However, the ^{27}Al$^+$ signal distribution across the multilayer (in the z-direction) indicates that the PVD-ALD deposition process has failed at some stage, i.e. the Al content is not only confined in the ALD layers but also spreads over one of the PVD layers. Therefore, the desired level of layer purity was not achieved in this case. To get more global view of this problem, the TOF-SIMS signals were integrated over x-y plane (Figure S5 and S6). These depth profiles reveal the presence of Al at the location of the Mo layer. This is an interesting observation as the process temperatures rather exclude the diffusion of elements between subsequent ALD and PVD cycles. The potential contamination of the Mo target is also rather unlikely as the ^{27}Al$^+$ signal does not appear in ZrMoAg layer,

which was fabricated by co-sputtering Mo, Zr and Ag targets. Besides, the signal at mass 27 cannot be assigned to any other element than Al as Al is the lightest element constituting the multilayer system. Furthermore, the potential atmospheric contaminants, such as H, C, N and O, usually ionize negatively and, therefore, do not appear in TOF-SIMS mass spectra acquired in the positive ion detection mode. This means that the presence of mass interference can be rather excluded in this case. The influence of potential porosity and columnar growth of PVD layers does not seem to determine the observation of Al at the location of Mo layer as SEM images on the sample cross-section (Figure S1b) show similar morphology of Mo and Zr layers (Al was not detected at the location of the Zr layer). Regardless of the origin of Al detection in the Mo layer, the TOF-SIMS data suggest the failure of the deposition process, i.e. not all deposited layers are pure and well-separated.

Furthermore, all three ALD thin films, deposited between the PVD layers, were designed to be exactly the same. However, if the thicknesses of Al_2O_3 layers were the same, the Full Width at Half Maximum (FWHM) of all $^{27}Al^+$ signal peaks would be the same, as the sputtering rates are identical. This is not the case as the estimated FWHM values vary between 5.6 and 7.3 frames. This indicates that the thicknesses of the ALD layers were different. It is worth mentioning that, the variations of the $^{27}Al^+$ signal peaks magnitudes (by 32% and 37% at frames 40 and 49, respectively, when compared to the highest $^{27}Al^+$ signal peak observed at frame 17) most likely result from the matrix effect and are rather not correlated with the thin film thicknesses. Furthermore, an unexpected, small (approx. 93% lower intensity than the maximum value) $^{27}Al^+$ signal peak was observed at the interface between the Zr layer and the Si substrate (at frame 77). A careful analysis of the deposition protocols revealed that most probably it originated from the RF plasma sputtering instrument, which was used for cleaning the Si substrate prior to the ALD-PVD depositions. It seems that the plasma simultaneously sputtered both, the sample substrate and the Al holder grid, on which the substrate was mounted, leading to the deposition of a minute amount of Al onto the Si surface. This is an important observation as, to our experience, no other analysis techniques (which are typically used for verifying quality of thin films, i.e. STEM/EDX and glow-discharge optical emission spectroscopy, GDOES), apart from TOF-SIMS, were able to detect such trace contamination.

In summary, a proper recognition of the deposition process failure requires the knowledge of the sample composition, including potential contaminants (as TOF-SIMS does not provide quantitative information), and certain level of expertise in the TOF-SIMS data analysis not to mistake it with mass interference- and matrix effect-related signal modifications. In summary, in the case of presented $ZrMoAg/Al_2O_3/Mo/Al_2O_3/Ag/Al_2O_3/Zr$ multilayer sample, the high sensitivity and high spatial resolution of TOF-SIMS allowed the detection of degradation in Mo layer purity and the inaccuracy of Al_2O_3 layer thicknesses despite a

very small quantity of Al content in the PVD-ALD multilayer sample. This demonstrates the potential of TOF-SIMS for the post-fabrication control of the multilayer quality, which is expected to help improving the thin film deposition protocols.

Very high sensitivity of TOF-SIMS: detection of deep-buried nanometre thick thin films

The easiest way to distinguish individual thin films in a multilayer stack during a TOF-SIMS analysis (assuming a lack of mass-interference) is based on representing the secondary ion signal distributions of the most prominent isotopes, which are present in different layers. Furthermore, in the case of multilayer systems based on multiple repetitive patterns of thin films, varying by a presence of one element (and, ideally, providing high mass contrast between the subsequent thin films), this element's secondary ion signal can be used for representing a sample structure. For example, a certified reference material for surface analysis, BAM-L200, whose upper part is made of alternating GaAs and $Al_{(0.70)}Ga_{(0.30)}As$ layers[65], was used to demonstrate ultrahigh lateral resolution (<20 nm) of a Bi_3 cluster TOF-SIMS instrument using only Al signal distribution[32]. In general, the recognition of layers becomes much more challenging as their components ionize weakly or these components ionize with different polarities (positive and negative) and, therefore, cannot be measured during a single TOF-SIMS measurement.

To demonstrate the very high chemical sensitivity of the TOF-SIMS technique, a difficult dedicated model $Al/Al_2O_3/Al/Al_2O_3/.../Al$ multilayer was deliberately chosen. In this case, the distinction of layers was expected to be challenging due to the fact that Al was present in all thin films and the subsequent layers varied only by the oxygen content. Furthermore, the two elements composing the sample usually do not appear in the same ion-detection mode, i.e. Al ionizes positively and O ionizes negatively. Besides, the thicknesses of Al_2O_3 layers were up to two orders of magnitude smaller than those of Al layers. Nonetheless, as presented in Figure 4, even such demanding sample structure can be chemically characterized using TOF-SIMS. Due to its extremely high sensitivity, solely the $^{27}Al^+$ signal distribution across the sample can be used to represent the location of pure Al layers and Al_2O_3 layers.

The normalized to 1 $^{27}Al^+$ signal depth profile (Figure S8a) perfectly demonstrates the differences in sputtering rates between the metallic (Al) and ceramic (Al_2O_3) layers. In the case of the uppermost Al/Al_2O_3 stack, the Al layer sputters almost seven times faster than the first Al_2O_3 layer (approx. 0.88 nm/frame vs. 0.13 nm/frame). Furthermore, the simultaneous delivery of fluorine gas to the sample surface during the FIB beam bombardment (Figure S8b) allowed for increasing the sputtering efficiency and, therefore, analyzing almost twice (7 layers instead of 4) as many layers as in the case of experiments without any gas in similar time, i.e. two Al and two Al_2O_3 thin films were
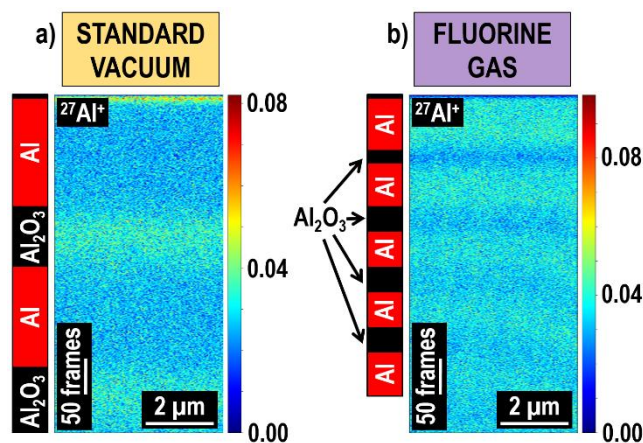
Figure 4. Elemental images of Al/Al$_2$O$_3$/Al/Al$_2$O$_3$/.../Al multilayer obtained with TOF-SIMS under standard vacuum conditions (a) and in the presence of fluorine gas (b). The ^{27}Al$^+$ signal distribution was sufficient to represent the location of metallic and ceramic thin films. Only the first few top layers of the multilayer (presented in Figure 1c) were measured. Note the inversion of Al ionization efficiency in the two experiments, i.e. ^{27}Al$^+$ signal is the highest at the Al$_2$O$_3$ layers during the measurements without gas and at the locations of Al thin films when fluorine gas is delivered.

measured during approx. 1h22min during the experiment conducted without any gas, whilst approx. 1h13min were needed to measure four Al and three Al$_2$O$_3$ layers during fluorine gas-assisted TOF-SIMS. The duration of the experimental time can be still reduced by increasing the primary ion beam energy and current, however usually this leads to the degradation of depth resolution[48] (note that the highest lateral resolution is achieved at the highest FIB beam energy of 30 keV, and the highest depth resolution is obtained at the low beam energies, i.e. usually ≤5 keV). The comparison of depth profiles obtained under different experimental conditions (with/without supplementary gas) show inverted tendency in the Al ionization efficiencies in the ALD and PVD layers. In the case of the measurements conducted under standard vacuum conditions (Figure S8a), the highest ^{27}Al$^+$ signal is observed within first several frames of the FIB sputtering process which is associated with the sample surface oxidation[47,49,53].

The increased ^{27}Al$^+$ signal is also used for the recognition of Al$_2$O$_3$ layers as oxygen increases the positive ion yields. This pattern is reversed in the case of results obtained during fluorine gas-assisted TOF-SIMS (Figure S8b), i.e. the amount of generated ^{27}Al$^+$ ions is the highest at the location of metallic layers. The ^{27}Al$^+$ depth profile given in the absolute values (not normalized) is shown in Figure S9. In the case of measurements performed without any gas, the signal peak associated to the native Al oxide, which spontaneously forms on the sample surface, is much higher than the signal peaks originating from the buried ALD-fabricated Al$_2$O$_3$ layers. This can potentially indicate different crystallinity[54] of these two aluminum oxides. The ^{27}Al$^+$ signal measured at the location of the Al$_2$O$_3$ layers is higher than Al signal measured at the locations of the pure Al layer (excluding the initial surface oxidation region) by a

factor of 1.3, i.e. approx. 6.5×10^{-4} counts·pixel^{-1}·pA^{-1} vs. 5×10^{-4} counts·pixel^{-1}·pA^{-1}. This shows the beneficial effect of oxygen on the Al ionization efficiency. Interestingly, in the case of results obtained during the fluorine-gas assisted TOF-SIMS, the first two Al layers give signals of approx. 7.2×10^{-4} counts·pixel^{-1}·pA^{-1} (measured at the signal plateaus) whilst the signal of 5.6-5.9×10^{-4} counts·pixel^{-1}·pA^{-1} was obtained at the locations of Al$_2$O$_3$ layers (factor of 1.2-1.3). Fluorine is the most electronegative element (i.e. 3.98 in the Pauling scale) in the periodic table and, therefore, its presence can modify interactions between metals and oxygen (for comparison, the electronegativity of oxygen is 3.44). This can potentially lead to the hampering of the ionization-enhancing effect of oxygen (which most likely caused the higher ^{27}Al$^+$ signal in Al$_2$O$_3$ layers during the TOF-SIMS measurements under standard vacuum conditions). In the conjunction with lower number of Al atoms in the Al$_2$O$_3$ layers than in the pure metal layers, this can explain the reversed shape of the ^{27}Al$^+$ depth profile obtained in the presence of fluorine gas. Remarkably, in the case of the fluorine gas-assisted TOF-SIMS measurements, the location of the deeply (approximately 530 nm, which is a lot for depth profiling, i.e. non-cross-sectional analysis, and taking into account low primary ion energy and low sputter rates of the ceramic) buried 4th (when counting from the sample surface) Al$_2$O$_3$ thin film with the thickness of approx. 8.5 nm can be well assessed. This is a very important result taking into account low sputter rates of the ceramic layers and the total sputtered depth. Usually, in such cases TOF-SIMS measurements are conducted on sample cross-sections or tomography[56,66] is performed. Both of these methods, however, are much more time-consuming due to the required sample preparation and provide lower resolution (as lateral resolution is lower than depth resolution). The difficulty in distinguishing the Al$_2$O$_3$ layers, which are buried deeper than the 4th layer (Figure 4b and S8b), most likely result from their decreasing thicknesses (i.e. each layer is thinner by approx. 1.21 nm than the upper one) and/or different amount of fluorine present on the bottom of the FIB-sputtered crater[49].

Conclusions

Thin films are broadly used in nanotechnologies, microelectronics, microdevices for new energy applications, medicine, as decorative layers, surface coatings etc. Since their optical/mechanical/electrical properties are determined by the chemical composition, the precise characterization techniques with nanoscale resolution are required. As presented in this study, the novel method of combining an *in situ* GIS with a HV-compatible TOF-SIMS detector allows the structure of thin film-based multilayer systems to be analysed fast with high sensitivity. The significant improvement of chemical image quality was achieved by injecting fluorine gas during the sputtering process. Furthermore, this solution allowed the mass interference between ions having similar masses to be separated, providing more representative data, when compared to the results obtained under standard vacuum conditions. Consequently, the structures of multilayer systems composed of thin films

with thicknesses varying between several nanometres to hundreds of nanometres were efficiently represented in 2D space (3D data representation is also possible with the current system but requires separate data reconstruction software[10]). As demonstrated, even layers, which are chemically very similar, can be well-distinguished due to the very high TOF-SIMS sensitivity. In the most extreme case of the $Al/Al_2O_3/Al/Al_2O_3/.../Al$ sample, the locations of approx. 12.1 nm, 10.1 nm, 10.8 nm and 8.5 nm thick Al_2O_3 layers, buried up to 530 nm deep below the surface, were assessed using only a single secondary ion signal distribution.

Currently, HV FIB/SEM is the most commonly system used for microanalysis and material science in research centres and industrial laboratories. This means that the chemical characterization with nanoscale resolution can be easily conducted on regular basis at a relatively low cost (comparing to the costs of dedicated UHV TOF-SIMS) by integrating HV-compatible TOF detectors. Furthermore, Ga FIB spot size can be as small as 2.5 nm at 1 pA ion current[67]. Although, so far the operation at such low ion currents was not practical for TOF-SIMS chemical analysis (due to the insufficient secondary ion generation), the recent advances in instrumentation[34] as well as in methodology[47-49] seem to indicate that this limitation can be overcome in the near future. Therefore, the presented technique is expected to play an important role in the development of thin film-based systems, verification of deposition process and potential failure analysis.

ASSOCIATED CONTENT

Supporting Information

Table S1. PVD deposition parameters of $Al_2O_3/Ni/Al_2O_3/Au/Al_2O_3/Cu/Al_2O_3$; Table S2: ALD deposition parameters of $Al_2O_3/Ni/Al_2O_3/Au/Al_2O_3/Cu/Al_2O_3$; Table S3. PVD deposition parameters of $ZrMoAg/Al_2O_3/Mo/Al_2O_3/Ag/Al_2O_3/Zr$; Table S4: ALD deposition parameters of $ZrMoAg/Al_2O_3/Mo/Al_2O_3/Ag/Al_2O_3/Zr$; Table S5. PVD deposition parameters of $Al/Al_2O_3/.../Al$; Table S6: ALD deposition parameters of $Al/Al_2O_3/.../Al$; Figure S1. The SEM images of mechanically cleaved cross-sections ; Figure S2. TEM results of $Al/Al_2O_3/.../Al/Al_2O_3/.../Al$; Figure S3. The depth profiles of $Al_2O_3/Ni/Al_2O_3/Au/Al_2O_3/Cu/Al_2O_3$; Figure S4. Normalized to 1 TOF-SIMS depth profiles of $Al_2O_3/Ni/Al_2O_3/Au/Al_2O_3/Cu/Al_2O_3$; Figure S5. TOF-SIMS depth profiles of the $ZrMoAg/Al_2O_3/Mo/Al_2O_3/Ag/Al_2O_3/Zr$ Figure S6. The normalized to 1 TOF-SIMS depth profiles of the $ZrMoAg/Al_2O_3/Mo/Al_2O_3/Ag/Al_2O_3/Zr$, Figure S7. The normalized to 1 TOF-SIMS depth profiles of signals acquired at masses 90, 106 and 107; Figure S8. The normalized to 1 depth profile of the $^{27}Al^+$ signal measured in $Al/Al_2O_3/.../Al$; Figure S9. The depth profile of $Al/Al_2O_3/.../Al$;

AUTHOR INFORMATION

Corresponding Author

* agnieszka.priebe@empa.ch

ACKNOWLEDGMENT

REFERENCES

(1)   Kumar, S.; Aswal, D. K. *Recent Advances in Thin Films*, 1st ed.; Springer, 2020.

(2)   Goswami, A. *Thin Film Fundamentals*; New Age Publications: New Dehli, 1996.

(3)   Frey, H.; Khan, H. R. *Handbook of Thin Film Technology*; Springer-Verlag Berlin Heidelberg: Berlin, Heidelberg, 2015. https://doi.org/10.1007/978-3-642-05430-3.

(4)   Constantin, R.; Miremad, B. Performance of Hard Coatings, Made by Balanced and Unbalanced Magnetron Sputtering, for Decorative Applications. *Surf. Coatings Technol.* **1999**, *120–121*, 728–733. https://doi.org/10.1016/S0257-8972(99)00366-7.

(5)   Navinšek, B.; Panjan, P.; Milošev, I. PVD Coatings as an Environmentally Clean Alternative to Electroplating and Electroless Processes. *Surf. Coatings Technol.* **1999**, *116–119*, 476–487. https://doi.org/10.1016/S0257-8972(99)00145-0.

(6)   Niinistö, L.; Päiväsaari, J.; Niinistö, J.; Putkonen, M.; Nieminen, M. Advanced Electronic and Optoelectronic Materials by Atomic Layer Deposition: An Overview with Special Emphasis on Recent Progress in Processing of High-k Dielectrics and Other Oxide Materials. *Phys. Status Solidi Appl. Res.* **2004**, *201* (7), 1443–1452. https://doi.org/10.1002/pssa.200406798.

(7)   Babu Krishna Moorthy, S. *Thin Film Structures in Energy Applications*; Springer International Publishing: Cham, Switzerland, 2015. https://doi.org/10.1007/978-3-319-14774-1.

(8)   Sastre, J.; Priebe, A.; Döbeli, M.; Michler, J.; Tiwari, A. N.; Romanyuk, Y. E. Lithium Garnet Li7La3Zr2O12 Electrolyte for All-Solid-State Batteries: Closing the Gap between Bulk and Thin Film Li-Ion Conductivities. *Adv. Mater. Interfaces* **2020**, *7* (17), 2000425. https://doi.org/10.1002/admi.202000425.

(9)   Sastre, J.; Lin, T.-Y.; Filippin, A. N.; Priebe, A.; Avancini, E.; Michler, J.; Tiwari, A. N.; Romanyuk, Y. E.; Buecheler, S. Aluminum-Assisted Densification of Cosputtered Lithium Garnet Electrolyte Films for Solid-State Batteries. *ACS Appl. Energy Mater.* **2019**, acsaem.9b01387. https://doi.org/10.1021/acsaem.9b01387.

(10)   Sastre, J.; Futscher, M. H.; Pompizi, L.; Aribia, A.; Priebe, A.; Overbeck, J.; Stiefel, M.; Tiwari, A. N.; Romanyuk, Y. E. Blocking Lithium Dendrite Growth in Solid-State Batteries with an Ultrathin Amorphous Li-La-Zr-O Solid Electrolyte. *chemrxiv* **2020**.

(11)   Lin, Y. *Advanced Nano Deposition Methods*, 1st ed.; Wiley-VCH: Weinheim, Germany.

(12)   Sterner, J.; Malmström, J.; Stolt, L. Study on ALD In2S3/Cu(In, Ga)Se2 Interface Formation. *Prog. Photovoltaics Res. Appl.* **2005**, *13* (3), 179–193. https://doi.org/10.1002/pip.595.

(13)   Platzer-Björkman, C.; Lu, J.; Kessler, J.; Stolt, L. Interface Study of CuInSe2/ZnO and Cu(In,Ga)Se2/ZnO Devices Using ALD ZnO Buffer Layers. *Thin Solid Films* **2003**, *431–432* (03), 321–325. https://doi.org/10.1016/S0040-6090(03)00229-3.

(14)   Kobayashi, T.; Kumazawa, T.; Jehl Li Kao, Z.; Nakada, T. Cu(In,Ga)Se2 Thin Film Solar Cells with a Combined ALD-Zn(O,S) Buffer and MOCVD-ZnO:B Window Layers. *Sol. Energy Mater. Sol. Cells* **2013**, *119*, 129–133. https://doi.org/10.1016/j.solmat.2013.05.052.

(15)   Bakke, J. R.; Pickrahn, K. L.; Brennan, T. P.; Bent, S. F. Nanoengineering and Interfacial Engineering of Photovoltaics by Atomic Layer Deposition. *Nanoscale* **2011**, *3* (9), 3482–3508. https://doi.org/10.1039/c1nr10349k.

(16)   Stefik, M.; Cornuz, M.; Mathews, N.; Hisatomi, T.; Mhaisalkar, S.; Grätzel, M. Transparent, Conducting Nb:SnO

2 for Host-Guest Photoelectrochemistry. *Nano Lett.* **2012**, *12* (10), 5431–5435. https://doi.org/10.1021/nl303101n.

(17) Yamada, A.; Sang, B.; Konagai, M. Atomic Layer Deposition of ZnO Transparent Conducting Oxides. *Appl. Surf. Sci.* **1997**, *112*, 216–222. https://doi.org/10.1016/S0169-4332(96)01022-7.

(18) Abb, M.; Sepúlveda, B.; Chong, H. M. H.; Muskens, O. L. Transparent Conducting Oxides for Active Hybrid Metamaterial Devices. *J. Opt. (United Kingdom)* **2012**, *14* (11). https://doi.org/10.1088/2040-8978/14/11/114007.

(19) Otto, M.; Kroll, M.; Käsebier, T.; Lee, S. M.; Putkonen, M.; Salzer, R.; Miclea, P. T.; Wehrspohn, R. B. Conformal Transparent Conducting Oxides on Black Silicon. *Adv. Mater.* **2010**, *22* (44), 5035–5038. https://doi.org/10.1002/adma.201002515.

(20) Martin, P. M. *Handbook of Deposition Technologies for Films and Coatings: Science, Applications and Technology*, 3rd ed.; Elsevier: Oxford, UK, 2010.

(21) Ortiz-Conde, A.; García Sánchez, F. J.; Liou, J. J.; Cerdeira, A.; Estrada, M.; Yue, Y. A Review of Recent MOSFET Threshold Voltage Extraction Methods. *Microelectron. Reliab.* **2002**, *42* (4–5), 583–596. https://doi.org/10.1016/S0026-2714(02)00027-6.

(22) Trolier-Mckinstry, S.; Muralt, P. Thin Film Piezoelectrics for MEMS. *J. Electroceramics* **2004**, *12* (1–2), 7–17. https://doi.org/10.1023/B:JECR.0000033998.72845.51.

(23) Eom, C. B.; Trolier-McKinstry, S. Thin-Film Piezoelectric MEMS. *MRS Bull.* **2012**, *37* (11), 1007–1017. https://doi.org/10.1557/mrs.2012.273.

(24) Shchekin, O. B.; Epler, J. E.; Trottier, T. A.; Margalith, T.; Steigerwald, D. A.; Holcomb, M. O.; Martin, P. S.; Krames, M. R. High Performance Thin-Film Flip-Chip InGaN-GaN Light-Emitting Diodes. *Appl. Phys. Lett.* **2006**, *89* (7), 2004–2007. https://doi.org/10.1063/1.2337007.

(25) Skoog, S. A.; Elam, J. W.; Narayan, R. J. Atomic Layer Deposition: Medical and Biological Applications. *Int. Mater. Rev.* **2013**, *58* (2), 113–129. https://doi.org/10.1179/1743280412Y.0000000009.

(26) Hovsepian, P. E.; Luo, Q.; Robinson, G.; Pittman, M.; Howarth, M.; Doerwald, D.; Tietema, R.; Sim, W. M.; Deeming, A.; Zeus, T. TiAlN/VN Superlattice Structured PVD Coatings: A New Alternative in Machining of Aluminium Alloys for Aerospace and Automotive Components. *Surf. Coatings Technol.* **2006**, *201* (1–2), 265–272. https://doi.org/10.1016/j.surfcoat.2005.11.106.

(27) Miller, M. k.; Kenik, E. a. Atom Probe Tomography: A Technique for Nanoscale Characterization. *Microsc. Microanal.* **2004**, *10* (03), 336–341. https://doi.org/10.1017/S1431927604040577.

(28) Williams, D. B.; Carter, C. B. The Transmission Electron Microscope. In *Transmission Electron Microscopy*; 1996. https://doi.org/10.1007/978-1-4757-2519-3_1.

(29) Volkert, C. A.; Minor, A. M. Focused Ion Beam Micromachining. *MRS Bull.* **2007**, *32* (May), 389–399. https://doi.org/10.1557/mrs2007.62.

(30) Benninghoven, A.; Rudenauer, F. G.; Werner, H. W. Secondary Ion Mass Spectrometry–Basic Concepts, Instrumental Aspects, Applications and Trends. *Surf. Interface Anal.* **1987**, *10* (8), 435. https://doi.org/10.1002/sia.740100811.

(31) Van de Heide, P. *Secondary Ion Mass Spectrometry: An Introduction to Principles and Practices*; 2014.

(32) Kollmer, F.; Paul, W.; Krehl, M.; Niehuis, E. Ultra High Spatial Resolution SIMS with Cluster Ions - Approaching the Physical Limits. *Surf. Interface Anal.* **2013**, *45* (1), 312–314. https://doi.org/10.1002/sia.5093.

(33) Alberts, D.; von Werra, L.; Oestlund, F.; Rohner, U.; Hohl, M.; Michler, J.; Whitby, J. A. Design and Performance of Two Orthogonal Extraction Time-of-Flight Secondary Ion Mass Spectrometers for Focused Ion Beam Instruments. *Instrum. Sci. Technol.* **2014**, *42* (4), 432–445. https://doi.org/10.1080/10739149.2013.878843.

(34) Priebe, A.; Barnes, J.-P.; Edwards, T. E. J.; Huszár, E.; Pethö, L.; Michler, J. Elemental Characterization of Al Nanoparticles Buried under a Cu Thin Film: TOF-SIMS vs STEM/EDX. *Anal. Chem.* **2020**, *92* (18). https://doi.org/10.1021/acs.analchem.0c02361.

(35) Huang, R.; Ikuhara, Y. STEM Characterization for Lithium-Ion Battery Cathode Materials. *Curr. Opin. Solid State Mater. Sci.* **2012**, *16* (1), 31–38. https://doi.org/10.1016/j.cossms.2011.08.002.

(36) Fearn, S. *An Introduction to Time-of-Flight Secondary Ion Mass Spectrometry (ToF-SIMS) and Its Application to Materials Science*; Morgan & Claypool Publishers: San Rafael, CA, USA, 2015. https://doi.org/10.1088/978-1-6817-4088-1.

(37) Sodhi, R. N. S. Time-of-Flight Secondary Ion Mass Spectrometry (TOF-SIMS):— Versatility in Chemical and Imaging Surface Analysis. *Analyst* **2004**, *129*, 483–487. https://doi.org/10.1039/B402607C.

(38) Whitby, J. A.; Östlund, F.; Horvath, P.; Gabureac, M.; Riesterer, J. L.; Utke, I.; Hohl, M.; Sedláček, L.; Jiruše, J.; Friedli, V.; Bechelany, M.; Michler, J. High Spatial Resolution Time-of-Flight Secondary Ion Mass Spectrometry for the Masses: A Novel Orthogonal ToF FIB-SIMS Instrument with in Situ AFM. *Adv. Mater. Sci. Eng.* **2012**, *2012*, 1–13. https://doi.org/10.1155/2012/180437.

(39) Pillatsch, L.; Östlund, F.; Michler, J. FIBSIMS: A Review of Secondary Ion Mass Spectrometry for Analytical Dual Beam Focussed Ion Beam Instruments. *Prog. Cryst. Growth Charact. Mater.* **2019**, *65* (1), 1–19. https://doi.org/10.1016/j.pcrysgrow.2018.10.001.

(40) Priebe, A.; Barnes, J.-P.; Edwards, T. E. J.; Pethö, L.; Balogh, I.; Michler, J. 3D Imaging of Nanoparticles in an Inorganic Matrix Using TOF-SIMS Validated with STEM and EDX. *Anal. Chem.* **2019**, *91*, 11834–11839 Article. https://doi.org/10.1021/acs.analchem.9b02545.

(41) Marin, E.; Guzman, L.; Lanzutti, A.; Fedrizzi, L.; Saikkonen, M. Chemical and Electrochemical Characterization of Hybrid PVD + ALD Hard Coatings on Tool Steel. *Electrochem. commun.* **2009**, *11* (10), 2060–2063. https://doi.org/10.1016/j.elecom.2009.08.052.

(42) Staszuk, M. Application of PVD and ALD Methods for Surface Treatment of Al-Si-Cu Alloys. *Solid State Phenom.* **2019**, *293*, 97–109. https://doi.org/10.4028/www.scientific.net/SSP.293.97.

(43) Xie, T.; Edwards, T. E. J.; Della Ventura, N.; Casari, D.; Huszár, E.; Fu, L.; Zhou, L.; Maeder, X.; Schwierdrzik, J.; Utke, I.; Michler, J.; Pethö, L. Synthesis of Model Al-Al2O3 Multilayer Systems with Monolayer Oxide Thickness Control by Circumventing Native Oxidation. *Thin Solid Films* **2020**, *711*, 138287. https://doi.org/https://doi.org/10.1016/j.tsf.2020.138287.

(44) Benninghoven, A. Chemical Analysis of Inorganic and Organic Surfaces and Thin Films by Static Time-of-Flight Secondary Ion Mass Spectrometry (TOF-SIMS). *Angew. Chem. Int. Ed. Engl* **1994**, No. 33, 1023–1043. https://doi.org/https://doi.org/10.1002/anie.199410231.

(45) Priebe, A.; Barnes Jean-Paul; Edwards, T. E. J.; Huszár, E.; Pethö, L.; Michler, J. Elemental Characterization of Al Nanoparticles Buried under a Cu Thin Film – TOF-SIMS vs. STEM/EDX. *Anal. Chem.* **2020**, *92*, 12518–12527. https://doi.org/10.1021/acs.analchem.0c0236.

(46) Nicolas, B.; Demers, H.; Gauvin, R. *Field Emission Scanning Electron Microscopy: New Perspectives for Materials Characterization*; Springer: Singapore, 2007.

(47) Priebe, A.; Utke, I.; Pethö, L.; Michler, J. Application of a Gas-Injection System during the FIB-TOF-SIMS Analysis - Influence of Water Vapor and Fluorine Gas on Secondary Ion Signals and Sputtering Rates. *Anal. Chem.* **2019**, *91* (18), 11712–11722. https://doi.org/10.1021/acs.analchem.9b02287.

(48) Priebe, A.; Pethö, L.; Michler, J. Fluorine Gas Coinjection as a Solution for Enhancing Spatial Resolution of Time-of-Flight Secondary Ion Mass Spectrometry and Separating

(49)   Mass Interference. *Anal. Chem.* **2020**, *92*, 2121–2129. https://doi.org/https://doi.org/10.1021/acs.analchem.9b046 47.

(49)   Priebe, A.; Xie, T.; Pethö, L.; Michler, J. Potential of Gas-Assisted Time-of-Flight Secondary Ion Mass Spectrometry for Improving Elemental Characterization of Complex Metal-Based Systems. *J. Anal. At. Spectrom.* **2020**, 35, 2997–3006. https://doi.org/https://doi.org/10.1039/D0JA00372G.

(50)   Wieczerzak, K.; Priebe, A.; Utke, I.; Michler, J. Practical Aspects of Focused Ion Beam Time-of-Flight Secondary Ion Mass Spectrometry Analysis Enhanced by Fluorine Gas Coinjection. *Chem. Mater.* **2021**, *33* (5), 1581–1593. https://doi.org/10.1021/acs.chemmater.1c00052.

(51)   Deline, V. R.; Katz, W.; Evans, C. A.; Williams, P. Mechanism of the SIMS Matrix Effect. *Appl. Phys. Lett.* **1978**, *33* (9), 832–835. https://doi.org/10.1063/1.90546.

(52)   Deline, V. R.; Evans, C. A.; Williams, P. A Unified Explanation for Secondary Ion Yields. *Appl. Phys. Lett.* **1978**, *33* (7), 578–580. https://doi.org/10.1063/1.90466.

(53)   Priebe, A.; Xie, T.; Bürki, G.; Pethö, L.; Michler, J. Matrix Effect in TOF-SIMS Analysis of Two-Element Inorganic Thin Films. *J. Anal. At. Spectrom.* **2020**, *35*, 1156–1166. https://doi.org/10.1039/C9JA00428A.

(54)   Vickermann, J. C.; Briggs, D. *ToF-SIMS: Materials Analysis by Mass Spectrometry*, 2nd ed.; IM Publications LLP: West Sussex, United Kingdom, 2013.

(55)   Priebe, A.; Audoit, G.; Barnes, J. P. A Novel PFIB Sample Preparation Protocol for Correlative 3D X-Ray CNT and FIB-TOF-SIMS Tomography. *Ultramicroscopy* **2017**, *173*, 10–13. https://doi.org/10.1016/j.ultramic.2016.11.010.

(56)   Priebe, A.; Bleuet, P.; Goret, G.; Laurencin, J.; Montinaro, D.; Barnes, J.-P. State-of-the-Art Three-Dimensional Chemical Characterization of Solid Oxide Fuel Cell Using Focused Ion Beam Time-of-Flight Secondary Ion Mass Spectrometry Tomography. *Microsc. Microanal.* **2016**, *22*, 1261–1269. https://doi.org/10.1017/S1431927616012502.

(57)   Utke, I.; Moshkalev, S.; Russell, P. *Nanofabrication Using Focused Ion and Electron Beams: Principles and Applications*; Utke, I., Moshkalev, S., Russell, P., Eds.; Oxford University Press: Oxford, 2012.

(58)   Moreno, M. A.; Mouton, I.; Chevalier, N.; Barnes, J.-P.; Bassani, F.; Gautier, B. Combined ToF-SIMS and AFM Protocol for Accurate 3D Chemical Analysis and Data Visualization. *J. Vac. Sci. Technol. B, Nanotechnol. Microelectron. Mater. Process. Meas. Phenom.* **2018**, *36* (3), 03F122. https://doi.org/10.1116/1.5019464.

(59)   Niehuis, E.; Moellers, R.; Kollmer, F.; Arlinghaus, H.; Bernard, L.; Hug, H. J.; Vranjkovic, S.; Dianoux, R.; Scheidemann, A. In-Situ TOF-SIMS and SFM Measurements Providing True 3D Chemical Characterization of Inorganic and Organic Nanostructures. *Microsc. Microanal.* **2014**, *20* (3), 2086–2087. https://doi.org/10.1017/S1431927614012161.

(60)   Pillatsch, L.; Kalácska, S.; Maeder, X.; Michler, J. In Situ Atomic Force Microscopy Depth-Corrected Three-Dimensional Focused Ion Beam Based Time-of-Flight Secondary Ion Mass Spectroscopy: Spatial Resolution, Surface Roughness, Oxidation. *Microsc. Microanal.* **2020**, No. 2020, 1–9. https://doi.org/10.1017/S1431927620024678.

(61)   Hamakawa, Y. *Thin-Film Solar Cells: Next Generation Photovoltaics and Its Applications*; Springer-Verlag Berlin Heidelberg: Berlin, 2004. https://doi.org/10.1007/978-3-662-10549-8.

(62)   Hagenhoff, B. High Resolution Surface Analysis by TOF-SIMS. *Mikrochim. Acta* **2000**, *132*, 259–271. https://doi.org/10.1007/s006040050019.

(63)   Kubicek, M.; Holzlechner, G.; Opitz, A. K.; Larisegger, S.; Hutter, H.; Fleig, J. A Novel ToF-SIMS Operation Mode for Sub 100 Nm Lateral Resolution: Application and Performance. *Appl. Surf. Sci.* **2014**, *289*, 407–416. https://doi.org/10.1016/j.apsusc.2013.10.177.

(64)   Peter, A.; de Paula, J. *Atkins' Physical Chemistry*; Oxford University Press: Oxford, 2014.

(65)   Senoner, M.; Maaßdorf, A.; Rooch, H.; Österle, W.; Malcher, M.; Schmidt, M.; Kollmer, F.; Paul, D.; Hodoroaba, V. D.; Rades, S.; Unger, W. E.S. Lateral Resolution of Nanoscaled Images Delivered by Surface-Analytical Instruments: Application of the BAM-L200 Certified Reference Material and Related ISO Standards. *Anal. Bioanal. Chem.* **2015**, *407* (11), 3211–3217. https://doi.org/10.1007/s00216-014-8135-7.

(66)   Priebe, A.; Goret, G.; Bleuet, P.; Audoit, G.; Laurencin, J.; Barnes, J. P. 3D Correlative Morphological and Elemental Characterization of Materials at the Deep Submicrometre Scale. *J. Microsc.* **2016**, *264* (2), 247–251. https://doi.org/10.1111/jmi.12458.

(67)   Fleck, R. A.; Humbel, B. M. *Biological Field Emission Scanning Electron Microscopy*; John Wiley & Sons, INC.: West Sussex, United Kingdom, 2019.